Cooperative Interaction between the Three Strands of a Designed Antiparallel β-Sheet

Gary J. Sharman and Mark S. Searle*

Contribution from the Department of Chemistry, University of Nottingham, University Park, Nottingham NG7 2RD, UK

Received February 20, 1997

Abstract: We describe the *de novo* design and characterization of a three stranded antiparallel β-sheet (peptide 1−24) and investigate the interplay between the two sets of weak interactions that occur at the interfaces between strands 1 and 2, and strands 2 and 3. We show by CD and NMR that peptide 1−24-folds into a three stranded sheet in aqueous methanol, and that the folded conformation of the C-terminal hairpin is more highly populated than the isolated β-hairpin (peptide 9−24). Both peptides have sigmoidal melting curves but a much broader transition is observed for the hairpin which also has a lower T_m (278K versus 298K); fitting to a two-state model gives the thermodynamic parameters for folding, which in both cases is enthalpy-driven. At 298K the three stranded sheet is ≈ 50% populated, while only ≈20% of the hairpin is folded. Despite a relatively small difference in stability between the sheet and hairpin, the former appears to have a much better defined structure in terms of both interstrand main chain and side chain interactions which we equate with a more extensive network of cooperative weak interactions. We have calculated an ensemble of 28 structures of the three-stranded β-sheet (backbone RMSD to the mean 1.3 ± 0.2 Å) using a combined torsion angle-driven distance geometry and molecular dynamics simulated annealing protocol, which reveal a right-handed twisted conformation consistent with β-sheets found in native proteins.

Introduction

Molecular recognition phenomena, including host−guest interactions in chemical systems and the processes by which complex chemical and biological structures self-assemble, are often fundamentally dependent on large numbers of weak noncovalent interactions and their cooperative interplay.[1−3] A desire to rationalize the forces involved in molecular complexation[4−6] and the stabilization of highly ordered molecular assemblies[7−11] has led to useful numerical estimates for assessing apparent binding contributions in molecular recognition studies.[6,11−13] Of necessity, these approaches are based on measuring the effects of localized structural modifications or mutations on overall stability constants. Cooperativity frequently complicates the analysis because specific changes in structure at one site can affect interactions elsewhere, reflecting some property of the whole set of linked weak interactions.[1−3,9,14−23] The corollary of this is that the binding energy between two entities in a bimolecular association may not simply be a property of the interactions at the interface between them, but may depend on changes to the internal structures and bonding of the associating entities concerned if they consist of extended arrays of weak interactions,[9,14−18] as typically found for a protein receptor. A recent example of this general principle is the promotion of glycopeptide antibiotic dimerization by the binding of model cell wall peptides.[1−3,14] Such cooperative effects are equally relevant to understanding protein folding initiation events, where elements of protein secondary structure of only marginal stability are likely to form as a consequence of local sequence preferences, and are subsequently consolidated and cooperatively stabilized as a consequence of interactions with other parts of the polypeptide chain.[24−28]

* Address correspondence to this author. Fax: 0115 951 3564. E-mail: mark.searle@nottingham.ac.uk.

(1) Westwell, M. S.; Searle, M. S.; Williams, D. H. *J. Mol. Recognit.* **1996**, *9*, 88−94.
(2) Williams, D. H.; Westwell, M. S. *Chem. Biol.* **1996**, *3*, 695−701.
(3) Williams, D. H.; Searle, M. S.; Westwell, M. S.; Mackay, J. P.; Groves, P.; Beauregard, D. A. *Chemtracts* **1994**, *7*, 133−159.
(4) Andrews, P. R.; Craik, D. J.; Martin, J. L. *J. Med. Chem.* **1984**, *27*, 1648−1657.
(5) Fersht, A. R. *Trends Biochem. Sci.* **1987**, *12*, 301−304.
(6) Searle, M. S.; Williams, D. H.; Gerhard, U. *J. Am. Chem. Soc.* **1992**, *114*, 10697−10704.
(7) Dill, K. A. *Biochemistry* **1990**, *29*, 7133−7155.
(8) Fersht, A. *Enzyme structure and mechanism*, 2nd ed.; W. H. Freeman and Company: New York, 1985.
(9) Serrano, L.; Horovitz, A.; Avron, B.; Bycroft, M.; Fersht, A. R. *Biochemistry* **1990**, *29*, 9343−9352.
(10) Shirley, B. A.; Stanssens, P.; Hahn, U.; Pace, C. N. *Biochemistry* **1992**, *31*, 725−732.
(11) Serrano, L.; Neira, J.-L.; Sancho, J.; Fersht, A. R. *Nature* **1992**, *356*, 453−455.
(12) Kellis, J. T.; Nyberg, K.; Fersht, A. R. *Biochemistry* **1989**, *28*, 4914−4922.
(13) Shortle, D.; Stites, W. E.; Meeker, A. K. *Biochemistry* **1990**, *29*, 8033−8041.
(14) Mackay, J. P.; Gerhard, U.; Beauregard, D. A.; Westwell, M. S.; Searle, M. S.; Williams, D. H. *J. Am. Chem. Soc.* **1994**, *116*, 4581−4590.
(15) Perutz, M. F. *Proc. R. Soc. London, Ser. B* **1980**, *208*, 135.
(16) Hua, Q. X.; Jia, W. H.; Frank, B. H.; Weiss, M. A. *J. Mol. Biol.* **1993**, *230*, 387−394.
(17) Serrano, L.; Bycroft, M.; Fersht, A. R. *J. Mol. Biol.* **1991**, *218*, 465−475.
(18) Horovitz, A.; Fersht, A. R. *J. Mol. Biol.* **1990**, *214*, 613−617.
(19) Adams, H.; Carver, F. J.; Hunter, C. A.; Morales, J. C.; Seward, E. M. *Angew. Chem., Int. Ed. Engl.* **1996**, *35*, 1542−1544.
(20) Kato, Y.; Conn, M. M.; Rebek, J. *J. Am. Chem. Soc.* **1994**, *116*, 3279−3284.
(21) Aoyama, Y.; Asakawa, M.; Matsui, Y.; Ogoshi, H. *J. Am. Chem. Soc.* **1991**, *113*, 6233−6240.
(22) Searle, M. S.; Sharman, G. J.; Groves, P.; Benhamu, B.; Beauregard, D. A.; Westwell, M. S.; Dancer, R. J.; Maguire, A. J.; Try, A. C.; Williams, D. H. *J. Chem. Soc., Perkin Trans. 1* **1996**, *23*, 2781−2786.

S0002-7863(97)00540-4 CCC: $15.00
Published on Web 05/15/1998

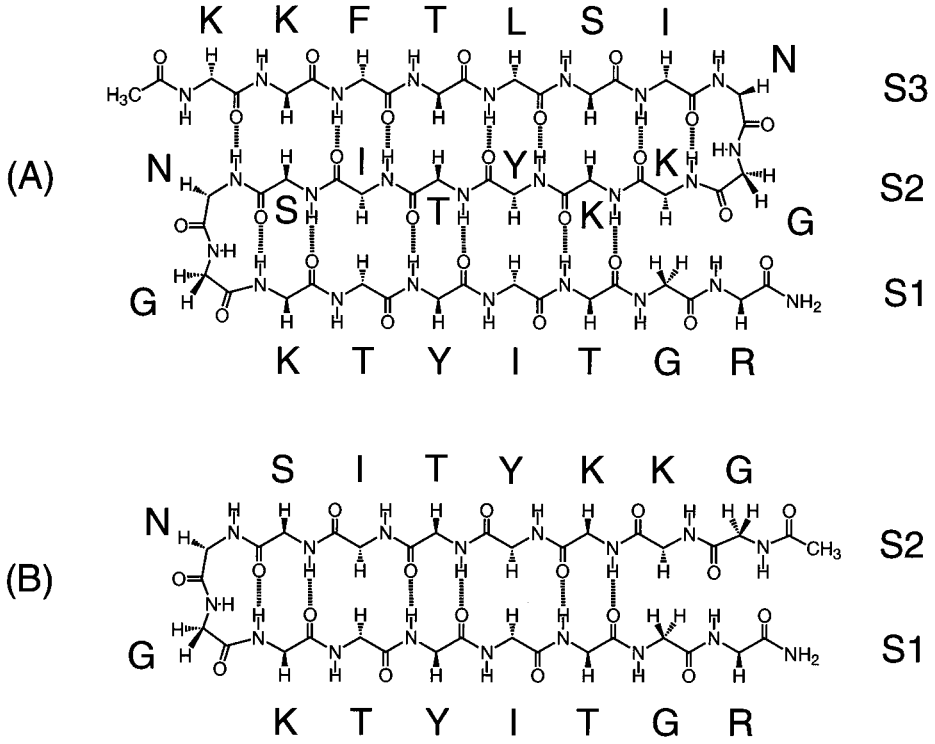

Figure 1. Residue sequence (K^1 K^2 F^3 T^4 L^5 S^6 I^7 N^8 G^9 K^{10} K^{11} Y^{12} T^{13} I^{14} S^{15} N^{16} G^{17} K^{18} T^{19} Y^{20} I^{21} T^{22} G^{23} R^{24}) and proposed register of hydrogen bonds for (A) the three stranded antiparallel β-sheet, peptide 1−24, β-strands S1, S2, and S3, and (B) the C-terminal β-hairpin, peptide 9−24, β-strands S1 and S2.

In the general context of understanding the nature of cooperative interactions in both chemical and biological molecular recognition processes, we describe a peptide system that has enabled us to investigate the interplay between two sets of weak interactions that occur at two different hydrogen bonded interfaces within a designed antiparallel three-stranded β-sheet (Figure 1). To dissect-out possible cooperative interactions we have synthesized two peptides. The first peptide (9−24) of 16 residues was designed to form a β-hairpin. The second peptide (1−24) ends with the same 16 residues but has a preceding 8 amino acid sequence designed to form a second β-turn and the third strand (S3) of the antiparallel β-sheet. The first strand (S1 in Figure 1) is in the same environment in both folded structures and undergoes the same changes in solvation and interstrand interactions when it interacts with S2. Thus, the indirect influence of the third strand on the stabilization of the interaction between S1 and S2 can be assessed in this system. We report here evidence from CD and NMR that 1−24 folds into a three-stranded sheet in which the C-terminal hairpin is cooperatively stabilized with respect to the isolated hairpin (9−24). We have calculated an ensemble of structures of the three-stranded sheet that are consistent with the NMR data.

Materials and Methods

Synthesis and purification of Peptides. Peptides were synthesized by using standard Fmoc solid-phase chemistry.[29,30] At the 16 residue stage of synthesis, half of the resin was removed, acetylated, and cleaved, while the remainder was carried through to give the 24 residue peptide. Both peptides were then purified by reverse phase HPLC on a C18 column (Waters, 10 mm × 100 mm). A flow rate of 8 mL min^{-1} was used, with isocratic buffer A for 5 min, followed by a linear gradient of 0 to 100% buffer B over 30 min (buffer A: water, 0.1% trifluoroacetic acid; buffer B: 30% water, 70% acetonitrile, 0.1% trifluoroacetic acid). The main fractions from successive runs were combined, evaporated under reduced pressure, redissolved in water, and lyopholized to give a white, fluffy powder. Electrospray mass spectrometry gave masses of 2760.0 (calculated 2760.2) and 1828.3 (calculated 1828.1) for the two peptides.

Peptide Aggregation. NMR chemical shifts and line widths were shown to be independent of peptide concentration in the range 5 mM to 50 μM, which strongly suggests, together with correlation times implied by temperature-dependent NOE intensities, that the peptide remains monomeric in solution at the concentration (≈2 mM) used for 2D NMR analysis.

Circular Dichroism (CD) Spectroscopy. CD spectra were acquired with an AVIV model 62DS spectrometer (Aviv Associates), using a 2 mm path length cell. Stock peptide solutions were prepared by weighing sufficient peptide to give 1 mL of 5 mM solution. Their pH was adjusted to 3.9 with HCl/NaOH solutions, before dilution with 2 mM NaH_2PO_4 buffer (pH 3.9), to give 50 μM solutions for analysis by CD. Typically 16 scans were acquired by using a 4 nm bandwidth from 250 to 190 nm with a step size of 1 nm. The resulting data were smoothed and baseline corrected. Spectra were also acquired with a bandwidth of 1 nm; these were identical except for significantly poorer signal to noise.

NMR Spectroscopy. All NMR experiments were performed on a Bruker DRX500 spectrometer on peptide samples of ≈2 mM concentration in D_2O or 90% H_2O/10% D_2O solution at pH 3.9 and 50% CD_3OD/50% D_2O or 50% CD_3OD/50% H_2O with the pH adjusted initially to 3.9 in aqueous solution. All chemical shifts are internally referenced to the sodium salt of trimethylsilylpropionate (TSP). Phase-sensitive DQF−COSY,[31] TOCSY,[32] NOESY,[33] and ROESY[34,35] experiments

(23) Sharman, G. J.; Searle, M. S.; Benhamu, B.; Groves, P.; Williams, D. H. *Angew. Chem., Int. Ed. Engl.* **1995**, *34*, 1483−1485.
(24) Fersht, A. R. *Proc. Natl. Acad. Sci. U.S.A.* **1996**, *92*, 10869−10873.
(25) Shortle, D. R. *Curr. Opin. Struct. Biol.* **1996**, *6*, 24−30.
(26) Freund, S. M. V.; Wong, K. B.; Fersht, A. R. *Proc. Natl. Acad. Sci. U.S.A.* **1996**, *93*, 10600−10603.
(27) Miranker, A. D.; Dobson, C. M. *Curr. Opin. Struct. Biol.* **1996**, *6*, 31−42.
(28) Smith, L. J.; Fiebig, K. M.; Schwalbe, H.; Dobson, C. M. *Folding Design* **1996**, *1*, R95−R106.
(29) Bodanszky, M.; Bodanszky, A. *The Practice of Peptide Synthesis*, 2nd ed.; Springer-Verlag: Berlin, 1994.
(30) Atherton, E.; Sheppard, R. C. In *Solid-phase peptide synthesis—practical approach*; Atherton, E., Ed.; IRL Press: Oxford, 1989.
(31) Piantini, U.; Sorensen, O. W.; Ernst, R. R. *J. Am. Chem. Soc.* **1982**, *104*, 6800−6801.

were performed at 283 K, collecting 2k points in f2 and 512 points in f1. Quadrature detection in f1 was achieved by using TPPI, and solvent suppression was achieved by presaturation. TOCSY experiments employed a spin locking field of 5 kHz, ROESY experiments 2 kHz. Mixing times of 100 and 200 ms were used in NOESY experiments. Data were processed on a Silicon Graphics Indy workstation with XWINNMR software. Typically, a sin-squared window function shifted by $\pi/3-\pi/2$ was applied in both dimensions, with zero filling in f1 to 1k points. For the measurement of coupling constants, high-resolution DQF−COSY and TOCSY with 8k points in f2 were used. Data were strip-transformed with zero filling to 32k in f2, using a Gaussian window function. Coupling constants were measured by deconvolution of extracted rows. One-dimensional spectra were acquired with 32k data points and processed with 1−2 Hz line broadening.

Structure Calculations. Starting structures were generated with DYANA 1.2.[36] A total of 75 upper limit distance restraints derived from NOEs were classified as strong (≤2.5 Å), medium (≤3.5 Å), and weak (≤5.0 Å). Only structurally useful intraresidue NOE restraints were included in calculations. In addition, 40 angle constraints, derived with HABAS from measured $^3J_{H\alpha-NH}$ coupling constants, were also applied (see Supporting Information). Where coupling constants could be measured (for 20 of the 24 residues) values were generally found to be larger (>7.5 Hz) than the residue-specific random coil values,[28] reflecting predominantly extended β-strand conformation. Thirty structures were annealed with 10 000 dynamics steps followed by 4 000 minimization steps. The three structures with the lowest target function values were then used as starting structures for molecular dynamics simulations with use of AMBER 4.1,[37] and the same set of distance and dihedral restraints. A variety of simulated annealing protocols were employed for the three different starting structures in order to generate an unbiased ensemble of structures which were independent of the starting conformers. Either 120 or 100 ps total simulation time was used according to the following protocol: (i) the temperature was increased from 1 K to 600 K over the first 30 ps, (ii) temperature was held constant for 20 ps, (iii) temperature was reduced to 300 K over 30 (25) ps, (iv) temperature was held at 300 K for 20 (15) ps, and (v) temperature was reduced to zero over 15 (10) ps and held at constant temperature for 5 (0) ps (numbers in parentheses refer to 100 ps dynamics). Distance and dihedral restraints were introduced over the first 2.5 ps by ramping the distance and torsional restraint force constants from 0 to 32 kcal mol^{-1} Å^{-2} and 0 to 32 kcal mol^{-1} rad^{-2}, respectively. Different random seeds were employed for each run, with starting velocities being assigned from a Maxwellian distribution at 50 K. Each run was performed both with and without bond lengths fixed by the SHAKE algorithm. A distance-dependent dielectric was used as an implicit water model. The resulting structures were analyzed with MOLMOL[38] and WHAT CHECK.[39] The coordinates of the final 28 structures, and those of the mean structure, are available on request from the authors.

Thermodynamic Analysis. By using the standard thermodynamic expressions

$$\Delta G^\circ = -RT \ln K \qquad \text{and} \qquad \Delta G^\circ = \Delta H^\circ - T\Delta S^\circ$$

and assuming a two state transition described by K = [folded]/[unfolded], the equilibrium constant K can be expressed in terms of the measured chemical shift difference $\Delta\delta$ between the Hε resonances of Y12 and Y20 at temperature T by

$$K = (\Delta\delta - \Delta\delta_U)/(\Delta\delta_F - \Delta\delta)$$

where $\Delta\delta_F$ and $\Delta\delta_U$ are the shift differences for fully folded and unfolded states, respectively. From these equations an expression can be derived for $\Delta\delta$ as a function of T in terms of ΔH° and ΔS° (at 298 K), where R is the gas constant:

$$\Delta\delta = \left\{\frac{\exp[-1/R(\Delta H^\circ/T - \Delta S^\circ)]}{1 + \exp[-1/R(\Delta H^\circ/T - \Delta S^\circ)]}\right\}(\Delta\delta_F - \Delta\delta_U) + \Delta\delta_U$$

Melting curves were fitted by using a nonlinear least-squares analysis within Kaleidagraph (Abelbeck software, version 2.1.3). The melting curve for the three-stranded sheet was well-defined by the data allowing ΔH°, ΔS°, $\Delta\delta_F$, and $\Delta\delta_U$ to be determined iteratively. The broader melting transition for the hairpin was less well defined and was fitted in two ways: first, with all parameters determined iteratively, as just described, and second, with the same limiting values for $\Delta\delta_F$ and $\Delta\delta_U$ determined for the longer peptide. Both methods fitted the experimental data equally well and resulted in very similar values for ΔH° (−39 and −34 kJ mol^{-1}) and for ΔS° (−139 and −123 J K^{-1} mol^{-1}). The numbers quoted in Table 1 represent the mean of these values with errors reflecting the uncertainty.

Table 1. ^{1}H NMR Assignment for Peptide 1−24, 50% (v/v) Methanol at 283 K

residue	HN	H_α	H_β	others
Lys 1	8.40	4.45	1.85, 1.70	H_γ 1.34, 1.45; H_δ 1.70; H_ϵ 2.98
Lys 2	8.47	4.70	1.57	H_γ 1.27; H_δ 1.38; H_ϵ 2.88
Phe 3	8.49	4.87	3.00, 3.18	H_δ 7.21; H_ϵ 7.30; H_ξ 7.30
Thr 4	8.33	4.69	3.99	H_γ 1.13
Leu 5	8.81	4.69	1.63	H_γ 1.63; H_δ 0.92
Ser 6	8.58	5.18	3.70, 3.80	
Ile 7	8.79	4.32	1.88	CH_3-H_γ 0.90; H_γ 1.1, 1.48; H_δ 0.75
Asn 8	9.13	4.52	2.82, 3.04	
Gly 9	8.62	3.67		H_α' 4.11
Lys 10	8.01	4.52	1.85, 1.70	H_γ 1.34, 1.45; H_δ 1.70; H_ϵ 2.98
Lys 11	8.32	4.81	1.85, 1.70	H_γ 1.34, 1.45; H_δ 1.70; H_ϵ 2.98
Tyr 12	8.85	4.68	2.88, 2.82	H_δ 7.00; H_ϵ 6.72
Thr 13	8.34	5.06	4.00	H_γ 1.17
Ile 14	8.32	4.84	1.64	CH_3-H_γ 0.80; H_γ 1.17, 1.40; H_δ 0.82
Ser 15	8.77	4.77	3.76	
Asn 16	9.12	4.57	2.99, 2.84	
Gly 17	8.72	3.71		H_α' 4.08
Lys 18	8.01	4.52	1.85, 1.70	H_γ 1.34, 1.45; H_δ 1.70; H_ϵ 2.98
Thr 19	8.16	4.64	3.95	H_γ 1.10
Tyr 20	8.85	4.75	3.00, 2.86	H_δ 7.08; H_ϵ 6.78
Ile 21	8.57	4.40	1.78	CH_3-H_γ 1.00; H_γ 1.15, 1.50; H_δ 0.87
Thr 22	8.46	4.87	3.91	H_γ 1.13
Gly 23	8.48	4.00		H_α' 4.00
Arg 24	8.34	4.35	1.76, 1.89	H_γ 1.66; H_δ 3.20

Results and Discussion

Design of a Three-Stranded β-Sheet Peptide. The sequence of the designed three-stranded β-sheet is that shown in Figure 1, and was chosen, in part, based on the statistical analysis of the protein data base (PDB) described by Ramirez-Alvarado et al.,[40] bearing in mind the need to maximize solubility and minimize peptide aggregation. The most abundant β-hairpins

(32) Braunschweiler, L.; Ernst, R. R. *J. Magn. Reson.* **1983**, *53*, 521−528.
(33) Jeener, J.; Meier, B. H.; Bachmann, P.; Ernst, R. R. *J. Phys. Chem.* **1979**, *71*, 4546−4553.
(34) Bax, A.; Davis, D. G. *J. Magn. Reson.* **1985**, *63*, 207−213.
(35) Bothner-by, A. A.; Stephens, R. L.; Lee, J.; Warren, C. D.; Jeanloz, R. W. *J. Am. Chem. Soc.* **1984**, *106*, 811−812.
(36) Güntert, P.; Mumenthaler, C.; Wüthrich, K. *J. Mol. Biol.* **1997**, *273*, 283.
(37) Pearlman, D. A.; Case, D. A.; Caldwell, J. W.; Ross, W. S.; Cheatham, T. E., III; Ferguson, D. M.; Siebel, G. L.; Singh, C.; Weiner, P. K.; Kollman, P. A. Amber 4.1; University of California, San Francisco, 1995.
(38) Koradi, R.; Billeter, M.; Wüthrich, K. *J. Mol. Graphics* **1996**, *14*, 51−55.
(39) Hooft, R. W. W.; Vriend, G.; Sander, C.; Abola, E. E. *Nature* **1996**, *381*, 272.
(40) Ramirez-Alvarado, M.; Blanco, F. J.; Serrano, L. *Nature Struct. Biol.* **1996**, *3*, 604−612.

in the PDB are those with two residue turns, with the type I′ variety being most common. Statistical analysis shows that the sequence Asn-Gly appears to be particularly favored.[41,42] Analysis of the ϕ,ψ distribution for residues in the coil regions of high-resolution protein X-ray structures[28,43] (that is, residues not found in regions of regular secondary structure) reveals that both Asn and Gly have a significant propensity (more so than for any other residue) to populate the left-handed (α_L) geometry required for a type I′ turn. Thus the free energy cost of restricting the backbone to a tight 2:2 type I′ turn[44] is particulalry low for this sequence. Recent analyses have examined the stability and conformational preferences of small model β-hairpin structures with different turn sequences.[45,46] Type I′ or II′ turns were shown to lead to the most stable hairpins with two-residue loops, but that type I and II are destabilizing within the same model hairpins.[45] For example, we have shown that altering the native bulged turn sequence in a ubiquitin-derived peptide to that of a two-residue type I turn sequence (Asn-Pro-Asp-Gly) is not compatible with the native hairpin conformation,[47] resulting in a bulged turn being reestablished with a (frame-shift) realignment of the two strands into a non-native conformation. The choice of the preferred type I′ turn also ensures that the hairpin has the necessary right-handed twist that is characteristic of protein β-sheets,[40,48,49] and which may be an important factor in the optimization of interstrand interactions and structure stabilization. As regards residues flanking the turn, Ramirez-Alvarado et al.[40] have pointed out that charged residues are particularly abundant at the position immediately following the Asn-Gly turn, while Val, Ile, Ser, and Tyr are common in the preceding position. We chose Ile-Asn-Gly-Lys and Ser-Asn-Gly-Lys for the two turns within the meander. In general, β-branched amino acids are found to have high β-sheet propensities[50−53] and were used liberally throughout the sequence. In addition, several studies of proteins, β-hairpin forming peptides, and α-helices have shown that side chain interactions between the aromatic ring of Tyr or Phe and Val, Ile, Leu, or Thr can lead to structure-stabilizing hydrophobic interactions[54,55] when these residues are opposite each other in interstrand hydrogen bonding positions.[56] Several interactions of this nature have been introduced through the incorporation of one Phe (Phe → Ile interaction) and two Tyr residues (Tyr → Leu and Tyr → Thr interactions). Thr has one of the highest intrinsic preferences for β-sheet formation[50−53] and two are often found opposite each other in non-hydrogen-bonding sites in antiparallel β-sheets;[57] such an interaction was introduced between strands 2 and 3 (see Figure 1). Two KK "doublets" were included to aid solubility but also to distribute positive charge over both faces of the designed β-sheet. In this way we avoided having one hydrophilic and one hydrophobic face, as is typically observed for peptides derived from native protein sequences, and hence minimized the possibility of peptide aggregation.

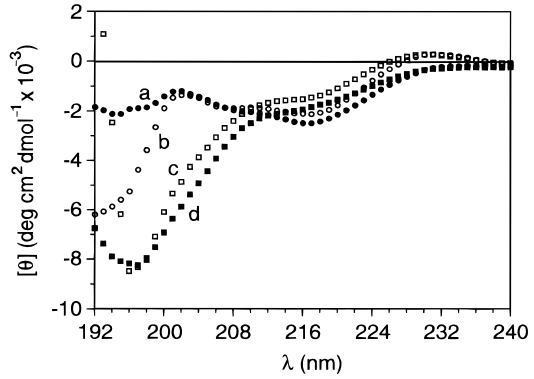

Figure 2. Far-UV CD spectra of peptides 1−24 and 9−24 at 298 K, 50 μM concentration: (a) 1−24 in 50% (v/v) aqueous methanol; (b) 9−24 in 50% (v/v) aqueous methanol; (c) 9−24 in water, pH 3.9; and (d) 1−24 in water, pH 3.9.

Conformational Analysis by Circular Dichroism Spectroscopy. CD spectroscopy provides a rapid and sensitive analysis of secondary structure propensity in peptides in solution.[58,59] Both meander and hairpin peptides were initially studied in aqueous solution at pH 3.9. Figure 2 shows the resulting CD spectra, which reveal both peptides to be essentially random coil, with similar molar ellipticity values at 196 nm, characteristic of a flexible conformation. The ellipticity of peptide 1−24 was subsequently investigated at a range of concentrations of methanol, and the aqueous/organic environment found to promote the formation of secondary structure. The CD spectrum in 50% (v/v) methanol showed a decrease in the negative ellipticity below 198 nm, but a more pronounced minimum around 216 nm characteristic of a substantial population of β-sheet and β-turn conformation. An isodichroic point at ca. 210 nm in the methanol titration (data not shown) suggested a two-state transition between folded and unfolded conformations. In contrast, the shorter peptide (9−24) exhibited rather smaller changes in molar ellipticity as the concentration of methanol increased (Figure 2), indicating a less marked transition to a folded structure in 50% (v/v) methanol, with much residual random coil still evident. A quantitative estimate of the population of folded structure present is described below.

Structural Analysis by ^{1}H NMR: (i) Perturbations to Hα Chemical Shifts. The deviation of ^{1}H NMR Hα chemical shifts from random coil values is a convenient method for establishing secondary structure formation since well-defined chemical shift changes are associated with extended β-strand and β-turn formation.[60,61] In agreement with the CD conclusions, both peptides showed very little evidence of folding in aqueous

(41) Hutchinson, E. G.; Thornton, J. M. *Protein Sci.* **1994**, *3*, 2207−2216.
(42) Sibanda, B. L.; Thornton, J. M. *J. Mol. Biol.* **1993**, *229*, 428−447.
(43) Swindells, M. B.; Macarthur, M. W.; Thornton, J. M. *Nature Struct. Biol.* **1995**, *2*, 596−603.
(44) Sibanda, B. L.; Thornton, J. M. *Methods Enzymol.* **1991**, *202*, 59−82.
(45) Haque, T. S.; Gellman, S. H. *J. Am. Chem. Soc.* **1997**, *119*, 2303−2304.
(46) deAlba, E.; Jimenez, M. A.; Rico, M. *J. Am. Chem. Soc.* **1997**, *119*, 175−183.
(47) Searle, M. S.; Williams, D. H.; Packman, L. C. *Nature Struct. Biol.* **1995**, *2*, 999−1006.
(48) Chou, K. C.; Nemethy, G.; Scheraga, H. A. *J. Mol. Biol.* **1983**, *168*, 389−407.
(49) Chothia, C. *J. Mol. Biol.* **1973**, *75*, 295−302.
(50) Minor, D. L.; Kim, P. S. *Nature* **1994**, *367*, 660−663.
(51) Minor, D. L.; Kim, P. S. *Nature* **1994**, *371*, 264−267.
(52) Kim, C. W. A.; Berg, J. M. *Nature* **1993**, *362*, 267−270.
(53) Smith, C. K.; Withka, J. M.; Regan, L. *Biochemistry* **1994**, *33*, 5510−5517.
(54) Padmanabhan, S.; Baldwin, R. L. *J. Mol. Biol.* **1994**, *241*, 706−713.
(55) Interactions appearing to stabilize β-conformation: (a) Kemmink, J.; Creighton, T. E. *J. Mol. Biol.* **1993**, *234*, 861−878. (b) Lumb, K. J.; Kim, P. S. *J. Mol. Biol.* **1994**, *236*, 412−420. (c) Dyson, H. J.; Sayre, J. R.; Merutka, G.; Shin, H.-C.; Lerner, R. A.; Wright, P. E. *J. Mol. Biol.* **1992**, *226*, 819−835.
(56) Smith, C. K.; Regan, L. Science **1995**, 270, 980−982.
(57) Wouters, M. A.; Curmi, P. M. G. *Proteins: Struct., Funct. Genet.* **1995**, *22*, 119−131.
(58) Johnson, W. C. *Annu. Rev. Biophys. Biophys. Chem.* **1988**, *17*, 145−166.
(59) Yang, J. T.; Wu, C. C.; Martinez, H. M. *Methods Enzymol.* **1986**, *130*, 208−269.
(60) Wishart, D. S.; Sykes, B. D.; Richards, F. M. *J. Mol. Biol.* **1991**, *222*, 311−333.

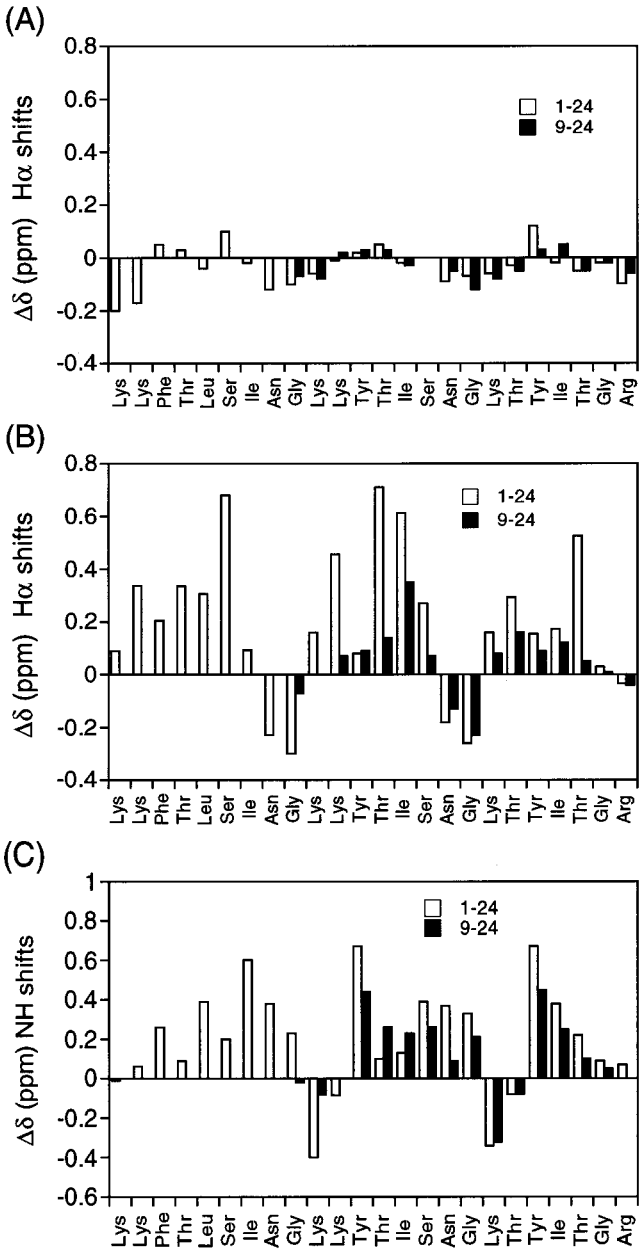

Figure 3. Summary of conformational shifts for peptides 1−24 and 9−24. Hα chemical shift deviations from random coil values ($\Delta\delta_{H\alpha}$ ppm) in (A) water, pH 3.9, at 283 K and (B) 50% (v/v) aqueous methanol at 283 K. (C) NH conformational shifts ($\Delta\delta_{NH}$ ppm) for both peptides in 50% (v/v) aqueous methanol at 283 K.

solution, with $\Delta\delta_{H\alpha}$ values (<0.1 ppm) falling below the chemical shift index proposed for identifying secondary structure in peptides and proteins (Figure 3A).[61] However, addition of methanol up to 50% (v/v) produced marked downfield changes in Hα chemical shifts with three contiguous segments of peptide 1−24 showing $\Delta\delta_{H\alpha}$ values significantly greater than 0.1 ppm (up to 0.7 ppm). These contiguous segments were interrupted by upfield shifted Hα resonances (≤0.3 ppm) for residues 8 and 9, and 16 and 17 (Figure 3B). The pattern of $\Delta\delta_{H\alpha}$ values is entirely consistent with three β-strands separated by two β-turns at the Asn 8-Gly 9 and Asn 16-Gly 17 steps. A full list of chemical shift assignments for peptide 1−24 in 50% (v/v) aqueous methanol at 283 K are presented in Table 1.

The calculation of $\Delta\delta_{H\alpha}$ values assumes that random coil chemical shifts determined in aqueous solution[62] are applicable in 50% methanol. To check this assumption, we have also studied an unrelated peptide of 20 residues of mixed sequence[63] which CD spectra and NMR analysis indicated as having a random coil conformation in 50% methanol. Chemical shift values in 50% aqueous methanol are in general slightly upfield of those in water. We have calculated an RMSD [$\delta_{(50\%MeOH)} - \delta_{(water)}$] of −0.02 (±0.03) ppm from the measured shifts of these peptides in the two solvents, and an RMSD from reported random coil values[62] in water of −0.03 (±0.04) ppm, indicating that solvation effects on chemical shifts were quite small. Therefore, $\Delta\delta_{H\alpha}$ values shown in Figure 3B were uncorrected for the change in solvent.

The truncated peptide 9−24 has been analyzed in 50% (v/v) methanol and the $\Delta\delta_{H\alpha}$ values obtained are plotted with those of 1−24 in Figure 3B. It is clear that the downfield shifts are significantly less marked for the isolated C-terminal sequence. Using the criteria outlined by Wishart et al.,[60,61] that segments of the peptide chain with ≥3 contiguous residues with chemical shift index >0.1 ppm can be identified as a β-strand, we are led to conclude that no segment of peptide 9−24 strictly satisfies the chemical shift index criteria for β-sheet formation. Notably, the Hα chemical shift of Ile 14 is shifted downfield by 0.38 ppm. In contrast, significant perturbations to the residues in the proposed turn region of peptide 9−24 are observed (Figure 3B), suggesting that the Asn 16-Gly 17 turn may be at least partially formed but that the association between the two strands is relatively weak. We are led to this conclusion since an important source of the downfield shift to the Hα resonance in the β-sheet has been shown to be the anisotropic contribution from the carbonyl group on the opposing strand,[64,65] making Hα shifts particularly sensitive to interstrand interactions. The overall pattern of $\Delta\delta_{H\alpha}$ values is generally consistent with a small population of β-hairpin structure in equilibrium with random coil. The clear qualitative conclusion from these data is that residues in strand 1, which are able to form the same hydrogen bonding pattern and side-chain interactions with strand 2 in both folded peptides, have a higher population of β-sheet conformation as part of the three-stranded sheet than they do in the isolated β-hairpin peptide.

(ii) Perturbations to NH Chemical Shifts. Although amide proton chemical shifts are not a reliable guide to the type of secondary structure present in the way Hα shifts are, it seemed that the size of $\Delta\delta_{NH}$ values for analogous residues in the two peptides could again provide a qualitative comparison of the extent of structure formation, since interstrand interactions are expected to provide a major contribution to the observed shifts. Again, this is particularly the case for residues in S1 which are in an identical environment in the folded structures of both peptides. The results show that the amide NHs are generally shifted downfield, with the exception of Lys 18 which immediately follows the turn. It is also clear that $\Delta\delta_{NH}$ values are generally larger for the meander (1−24) than for the hairpin (9−24) (Figure 3C), again reflecting the larger population of folded structure for these residues in the meander than the hairpin. The notable exceptions are the NHs of Thr 13 and Ile

(61) Wishart, D. S.; Sykes, B. D.; Richards, F. M. *Biochemistry* **1992**, *31*, 1647−1651.

(62) Wüthrich, K. *NMR of proteins and Nucleic acids*; Wiley: New York, 1986; p 17.

(63) The peptide studied was a 20 amino acid fragment derived from the N-terminus of the B1 domain of protein L. The sequence was VTIKANLITPSGTQTAEFKG. The calculated RMS Hα chemical shift deviation from the random coil values of Wuthrich[62] excludes T9 which has an anomalous shift due to the neighboring proline.

(64) Osapay, K.; Case, D. A. *J. Biomol. NMR* **1994**, *4*, 215−230.

(65) Unpublished results (Sharman, G. J.; Maynard, A. J.; Searle, M. S., in preparation) on model β-hairpin peptides and analysis of NMR data from available PDB structures shows this to be the case.

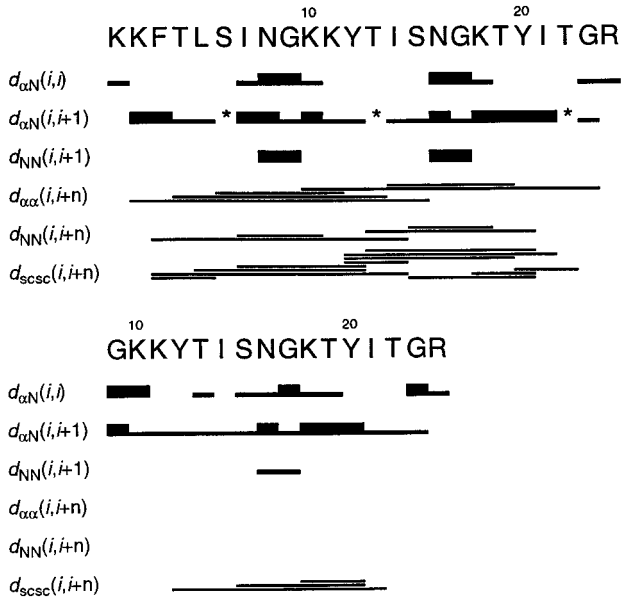

Figure 4. Summary of NOE intensities and long-range interactions for peptides 1−24 and 9−24 in 50% (v/v) aqueous methanol at 283 K. Asterisks indicate NOEs that could not be clearly resolved. The thickness of the bars reflects the intensity of the NOE observed (strong <3.0 Å, weak >3.0 Å) in the case of intraresidue and sequential interactions.

14 which have smaller downfield shifts in the longer peptide, which we assume are influenced by the ring current effects from one or a combination of aromatic side chains (Phe 3, Tyr 12, and Tyr 20) which are in reasonably close proximity to these residues, as suggested by side chain NOEs (see below). Lys 18 NH shows a similarly large upfield shift for both peptides which again seems to point to the turn region in both cases being equally well formed.

(iii) Conformational Analysis from NOE Data. A recent description of the random coil conformation from a statistical analysis of ψ,ϕ distributions in the coil regions of protein high-resolution X-ray structures[43] has led to a population-weighted description of backbone torsion angles from which both short-range and medium-range NOEs can be calculated.[28,66] This population-weighted random coil model provides a useful reference state for identifying deviations indicative of local structure formation in peptides, protein fragments, and denatured states of proteins. In this model, all sequential Hα-NH and NH-NH NOEs [abbreviated as αN(i,i+1) and NN(i,i+1), respectively] are predicted to be observed, reflecting significant populations of both α and β conformers for each residue in the random coil. The ratio of intensities αN(i,i+1)/NN(i,i+1) is shown to have an average value of ≈1.4, although this ratio is dependent on the residue-specific ψ,ϕ population; excluding Gly, this varies between 1 (Asn) and 2.7 (Ile).[66] The ratio is significantly different when residues adopt predominantly β-strand conformation.[28] The average ratio of intensities αN(i,i+1)/NN(i,i+1) increases dramatically to ≈55 for the regular β-sheet secondary structure found in proteins. We have carried out an analysis of NOE intensities for peptides 1−24 and 9−24 using NOESY data collected at 283 K (Figure 4). The NN(i,i+1) NOEs are not detected for the residues of the meander, except for Asn 8 → Gly 9 and Asn 16 → Gly 17 in the turn regions (see below), while αN(i,i+1) NOEs are medium/strong (Figure 5). This is clearly indicative of a high αN(i,i+1)/NN(i,i+1) intensity ratio, which we estimate to be >16 by integrating areas where an NN(i,i+1) peak might have been expected. This is clearly consistent with a predominantly extended β-strand conformation rather than random coil. Where $^3J_{H\alpha-NH}$ coupling constants could be measured (for 20 of the 24 residues), values were generally found to be larger (>7.5 Hz) than the residue-specific random coil values,[28] also reflecting residues in predominantly extended β-strand conformation. In the turn regions, however, NN(i,i+1) NOEs are observed, giving an αN(i,i+1)/NN(i,i+1) ratio close to 1 for Asn 8 → Gly 9 and Asn 16 → Gly 17.

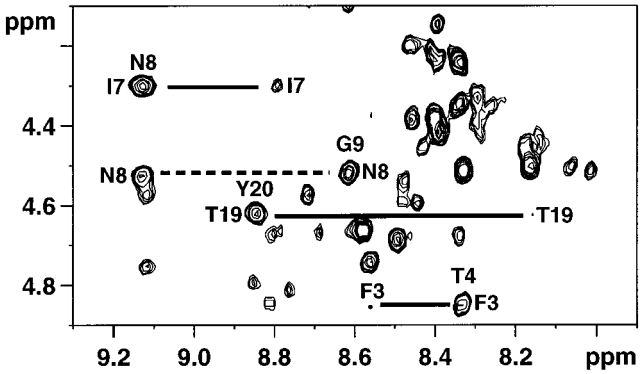

Figure 5. Portion of the Hα-NH region of the 200 ms NOESY spectrum of peptide 1−24 in 50% (v/v) aqueous methanol (H_2O/CD_3-OD) at 283 K. Pairs of αN(i,i+1) and αN(i,i) NOEs are highlighted for residues F3, I7, N8, and T19. Solid lines connect cross-peaks for residues in extended β-strands (F3, I7, and T19), while a dotted line connects the NOEs of N8 in the first turn region.

The NOE intensity ratio αN(i,i+1)/αN(i,i) provides a further handle on the population of β-conformers present in solution. Using the same set of 85 high-resolution structures described in the earlier analysis by Fiebig et al.,[66] we have estimated the αN(i,i+1)/αN(i,i) NOE intensity ratio in the random coil using the ψ,ϕ distribution from the coil regions. A value of ≈2.3 is predicted for the population-weighted random coil model, but generally larger values of >4 are predicted for a β-sheet. We measure from the same NOESY data sets values ranging between 4 and 9 for residues in the β-strands, again consistent with a very high proportion of extended β-structure in the meander. The relative intensities of αN(i,i+1) and αN(i,i) NOEs are highlighted for Phe 3, Ile 7, and Thr 19 in Figure 5, with intraresidue connectivities barely visible above the noise level. Again, significant deviations from these intensity ratios are apparent for Asn 8 → Gly 9 and Asn 16 → Gly 17 that reflect the involvement of these residues in β-turns. Here the αN(i,i+1)/αN(i,i) NOE intensity ratio is also close to 1 (evident for Asn 8 in Figure 5), consistent with the (left-handed) α_L population of Asn 8, Gly 9, Asn 16, and Gly 17 required for type I′ turns.

The population weighted random coil model also predicts the observation of medium range NOEs such as αN(i,i+2) and αN-(i,i+3), as a consequence of the presence of a significant population of $\beta(i)\alpha(i+1)$ and $\alpha(i)\alpha(i+1)$ conformers,[28,66] and these have been observed in protein fragments and urea denatured states of proteins. No such NOEs are observed for the meander, which is consistent with the predominance of the $\beta(i)\beta(i+1)$ conformation of an extended β-strand.

The general features described above for peptide 1−24 also seem to be apparant for the hairpin peptide 9−24 (Figure 4). NN(i,i+1) NOEs are similarly not detected within the proposed strand regions, reflecting a predominance of the extended β-strand conformation, while NN(i,i+1) NOEs corresponding to Asn 16 → Gly 17 in the turn are evident. The αN(i,i+1)/

(66) Fiebig, K. M.; Schwalbe, H.; Buck, M.; Smith, L. J.; Dobson, C. M. *J. Phys. Chem.* **1996**, *100*, 2661−2666.

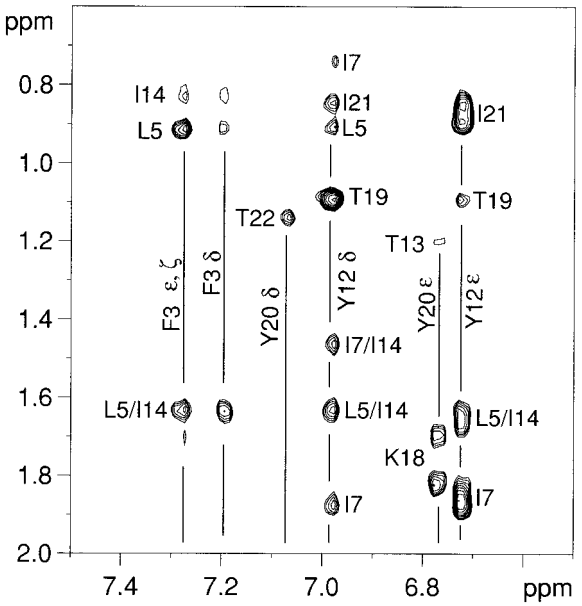

Figure 6. Portion of the 200 ms NOESY spectrum of peptide 1−24 in 50% (v/v) aqueous methanol at 283 K highlighting long-range NOEs and *i*,*i*+2 interactions involving the aromatic side chain protons of F3, Y12, and Y20 and aliphatic residues, as labeled.

αN(*i*,*i*) NOE intensity ratio is again generally high within the strands, but close to one in the turn region.

The observation of long-range NOEs is generally considered to provide the most conclusive evidence for the formation of the folded structure in solution. For peptide 1−24, many intense interstrand Hα → Hα, NH → NH interactions were readily detected between residues of S1 and S2, and between those of S2 and S3, that are fully consistent with the proposed antiparallel alignment and register of the peptide backbone shown in Figure 1. The NOE data are summarized in Figure 4. These included many of the expected cross-strand Hα → Hα NOEs (K2 → S15, T4 → T13, S6 → K11, K10 → G23, I14 → T19) and NH → NH NOEs (F3 → I14, I7 → K10, T13 → Y20, S15 → K18), although the observation of several additional predicted interactions was precluded by Hα or NH chemical shift degeneracies. A further significant number of interactions were observed between side chains in close proximity (for example, F3 → I14; Y12 → L5/I7/T19/I21 and Y20 → T13/S15). Many of these long-range NOEs, involving aromatic side chains, are illustrated in the portion of the NOESY spectrum shown in Figure 6. In addition, a number of *i*,*i*+2 NOEs between side chains are also apparent in Figure 6 (F3 → L5; Y12 → I14 and K18 → Y20 → T22); however, NOEs between the side chains of neighboring residues (*i*,*i*+1) are not generally observed, consistent with a contiguous extended β-strand conformation in which alternate residues along the sequence lie on the same face of the β-sheet.

In contrast to the large number of NOEs identified between main chain Hα and NH of the antiparallel β-strands of the meander, no long-range Hα → Hα or NH → NH interactions were observed for the shorter peptide. Both NOE and ROE data were collected at different temperatures and mixing times to eliminate the possible effects of differences in correlation times between the two peptides on the intensities of NOEs and cross-relaxation rates. Despite the lack of main chain interactions, analoguous Y12 → I21 and Y20 → S15 side chain interactions were evident, suggesting a disordered structure stabilized by a rather limited number of persistent side chain interactions. The absence of main chain interstrand NOEs would seem to preclude stabilization of the hairpin by the hydrogen bonding interactions normally associated with "regular" secondary structure. The much larger number of long-range NOEs observed for the meander appears to reflect more persistent side chain interactions held in much closer proximity as a consequence of such a hydrogen bonding framework.

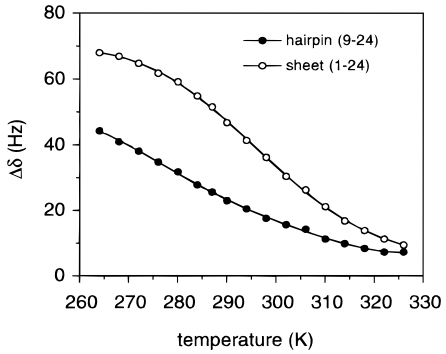

Figure 7. Melting curves for peptides 1−24 and 9−24 in 50% (v/v) aqueous methanol determined by NMR from the temperature dependence of the chemical shift difference (Δδ in Hz) between the Hε resonances of Y12 and Y20. The data were fitted to a two-state model by using a nonlinear least-squares analysis enabling Δ*H*° and Δ*S*° for folding to be determined (see Table 1). The lines of best fit to the data are shown; the correlation coefficient (*R*) in each case is >0.99 (see Methods).

Table 2. Thermodynamic Data (Δ*H*°, Δ*S*° and Proportion of Folded Structure, P_β) for Folding in 50% v/v Methanol Determined by van't Hoff Analysis of Melting Profiles

peptide	Δ*H*° (kJ mol^{-1})	Δ*S*° (J K^{-1} mol^{-1})	P_β (298 K)
β-sheet (1−24)	−60 (±2)	−201 (±7)	0.51
β-hairpin (9−24)	−36 (±4)	−131 (±12)	0.22

Van't Hoff Analysis of Peptide Stability. The change in folded population with temperature has been examined for both peptides by monitoring the chemical shift difference between the Hε aromatic protons of Y12 and Y20 ($\Delta\delta = \delta_{Y12} - \delta_{Y20}$), whose chemical shifts diverge as the temperature is lowered and the peptides fold, but converge to approximately the same limiting chemical shift in the fully unfolded state (Figure 7). Both peptides show sigmoidal melting profiles, although the limiting shift values for the hairpin (9−24) were not fully defined within the accessible temperature range. A significantly sharper transition is observed for peptide 1−24 reflecting the larger number of weak interactions stabilizing the structure. The "*n*" effect[1,2] observed here is reminiscent of the change in DNA or RNA melting profile that occurs as the number of interacting units ("*n*" base pairs) increases.[67] Not only is the melting profile sharper for the three-stranded sheet but it also has a higher midpoint transition temperature (298 K versus 278 K), indicating a higher overall stability.

Standard thermodynamic expressions have been used to derive an equation relating the difference in chemical shift Δδ as a function of temperature (*T*) to Δ*H*° and Δ*S*° (298 K) for folding. We made two assumptions: (i) that folding was a two-state process, supported by the CD data that show an isodichroic point at 210 nm when the peptide is titrated with methanol, and (ii) Δ*H*° and Δ*S*° for folding were temperature independent (i.e., $\Delta C_p^\circ \approx 0$; see below). Using a nonlinear least-squares curve fitting procedure (see methods), we have determined values for Δ*H*° and Δ*S*° enabling the population of folded structure to be calculated at 298 K (Table 2). The iterated curves fit extremely well to the experimental data (Figure 7), with

(67) Porschke, D. *Biopolymers* **1971**, *10*, 1989−2013.

correlation coefficients in both cases of >0.99, suggesting that the two-state model is a reasonable approximation. The analysis shows that at 298 K peptide 1−24 is ≈50% folded, while only ≈20% of the hairpin conformation is populated by peptide 9−24.

In both cases, folding is shown to be enthalpy driven (Table 2), with $\Delta G°$ for folding at 298 K representing a small difference between compensating large negative enthalpy and entropy terms. Thermodynamic studies of the folding of a model β-hairpin peptide[68] and native ubiquitin[69] in both water and methanolic solutions, using van't Hoff and calorimetric analysis, respectively, indicate that the hydrophobic contribution to folding is negligible since the solvent-ordering component of the hydrophobic effect is absent ($\Delta C_p° \approx 0$) under similar solvent conditions to those described here (50% v/v methanol). The thermodynamic parameters in Table 2 concur with the generally held view that organic solvents stabilize secondary structure by promoting intramolecular hydrogen bonding (electrostatic interactions) at the expense of weaker amide−solvent interactions,[70−73] suggesting an enthalpy-driven mechanism offset by an adverse conformational entropy term for ordering the peptide backbone.[68] Consistent with the greater number of interstrand stabilizing interactions in the three-stranded sheet, both $\Delta H°$ and $\Delta S°$ were significantly larger than for the hairpin (Table 2). However, enthalpy−entropy compensation[74] resulted in a relatively small difference in stability between the three-stranded sheet and β-hairpin at 298 K ($\Delta\Delta G° \approx 3$ kJ mol^{-1}), reflecting a difference in the population of hairpin versus sheet of only a factor of ≈2. Despite such a small difference in stability, the main chain alignment and abundance of side chain interactions implied by the NOE data all point to the sheet adopting a more ordered structure with a persistent hydrogen bonded framework.

Structure of a Three-Stranded Antiparallel β-Sheet. Conformational averaging precludes a rigorous interpretation of the NOE and coupling constant data in terms of a unique structure, but it is nevertheless useful to calculate an ensemble of structures compatible with the experimental restraints to identify the general features of the folded conformation. We have restricted our analysis to the folded structure of peptide 1−24, which adopts a high population (≈80%) of the three-stranded antiparallel β-sheet in solution at 283 K. A significant number of long-range interactions involving main chain Hα and NH NOEs are observed at this temperature, consistent with a conformation with persistent interstrand hydrogen bonding interactions. This is in contrast to the C-terminal hairpin, which in isolation shows no main chain long-range interactions.

Initially, a set of 30 structures were generated by using the torsion angle-driven distance geometry approach of DYANA.[36] A total of 75 upper-limit distance restraints were used, classified into the three categories strong, medium, and weak, together with 40 torsion angle constraints derived from three-bond coupling constants. Three of the 30 structures with the lowest target function values were then subjected to a simulated annealing protocol within AMBER 4.1 (see methods).[37] Several different dynamics protocols were used, including different random starting velocities, leading to an ensemble of 28 final structures showing similar backbone RMSD values to the mean structure of 1.3 ± 0.2 Å (all heavy atom RMSD to the mean of 2.1 ± 0.2 Å). Various structural statistics are shown in Table 3, including RMS deviations from experimental distance and dihedral restraints. The ϕ,ψ distribution plot (Figure 8) shows that 99% of residues lie in favored regions of the Ramachandran plot as determined by WHATCHECK.[39] The mean structure showed all of the expected backbone hydrogen bonds with recognized bond lengths and geometries.

Table 3. Structural Statistics for the Final 28 Refined MD Structures from 100 or 120 ps Restrained Dynamics Using AMBER 4.1

backbone rmsd from mean[a]	1.3 ± 0.2 Å
heavy atom rmsd from mean[a]	2.1 ± 0.2 Å
rms deviations from exptl distance restraints[b]	0.025 ± 0.002 Å
rms deviations from exptl dihedral restraints[b]	1.0 ± 0.1 deg
ω angle standard deviation[c]	6 ± 1 deg
deviations from ideal covalent[c]	
bonds	0.014 ± 0.001 Å
torsions	1.91 ± 0.09 deg
% age residues in favorable regions of the ramachandran plot	57% in most favorable[d] 99% in favorable + additional[d] 96% in allowed space[e]

[a] For residues 2−25, calculated by MOLMOL. [b] Over the final 1 ps of dynamics. [c] Calculated for nonshake structures using WHAT CHECK.[39] [d] Areas defined by WHATCHECK.[39] [e] Area as defined in MOLMOL.[38]

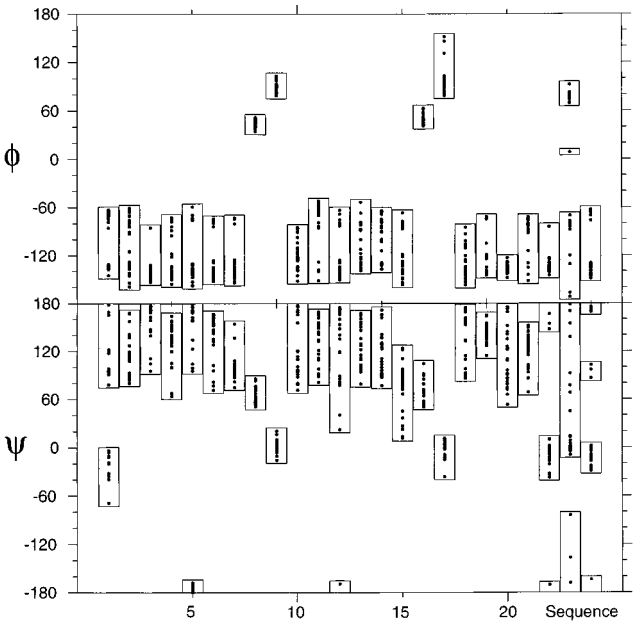

Figure 8. ϕ,ψ distribution plot for all residues of the 28 final structures determined for the three-stranded β-sheet. Each dihedral angle is indicated by a dot. The diagrams were generated by MOLMOL.[38]

The ensemble of 28 overlayed structures (backbone only) are shown in stereo in Figure 9A, while the mean structure is shown as a ribbon structure in Figure 9B. The three strands of the antiparallel β-sheet are connected by two type I′ turns, which are well-defined by the NOE data, with Asn 8 and 16 occupying the left-handed (α_L) region of conformational space (Figure 8). Noticably, the three-stranded sheet has the characteristic right-handed twist (see Figure 9B) exhibited by most protein β-sheets.[48,49] Thus a combination of experimental restraints and

(68) Maynard, A. J.; Sharman, G. J.; Searle, M. S. *J. Am. Chem. Soc.* **1998**, *120*, 1996−2007.
(69) Woolfson, D. N.; Cooper, A.; Harding, M. M.; Williams, D. H.; Evans, P. A. *J. Mol. Biol.* **1993**, *229*, 502−511.
(70) Nelson, J. W.; Kallenbach, N. R. *Proteins* **1986**, *1*, 211.
(71) Arakawa, T.; Goddette, D. *Arch. Biochem. Biophys.* **1985**, *240*, 21−32.
(72) Storrs, R. W.; Truckses, D.; Wemmer, D. E. *Biopolymers* **1992**, *32*, 1695−1702.
(73) Sonnichsen, F. D.; Van Eyk, J. E.; Hodges, R. S.; Sykes, B. D. *Biochemistry* **1992**, *31*, 8790−8798.
(74) Searle, M. S.; Westwell, M. S.; Williams, D. H. *J. Chem. Soc., Perkin Trans. II* **1995**, 141−151.

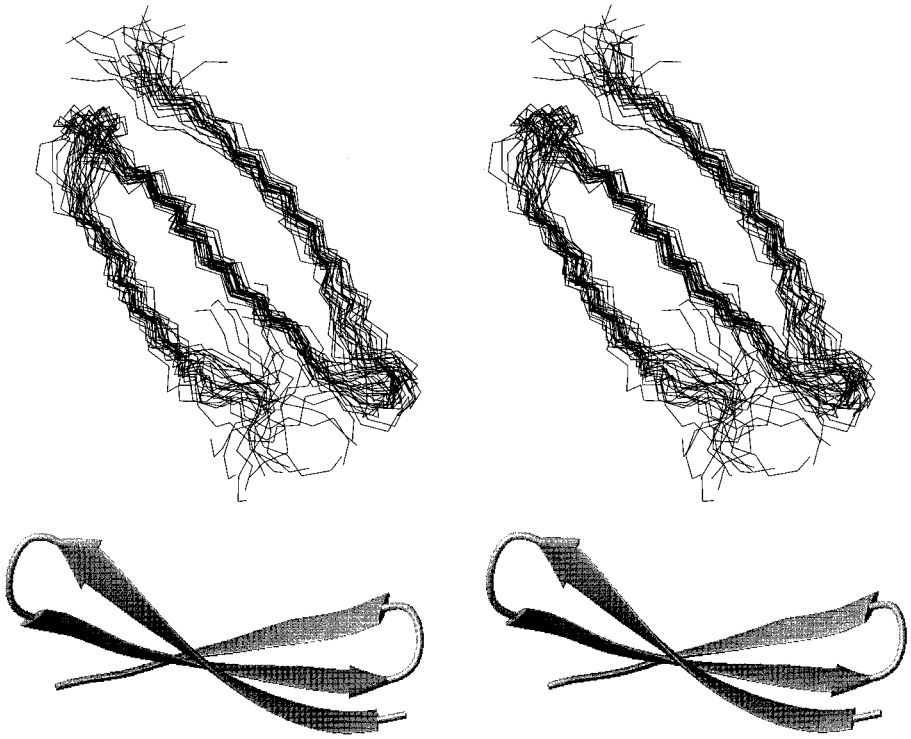

Figure 9. Stereoplots of 28 overlayed structures (backbone only) illustrating the antiparallel fold of the three strands, and a ribbon diagram of the mean structure (edge on view) highlighting the twisted conformation of the three strands of the sheet. The diagrams were generated by MOLMOL.[38]

the AMBER 94 force field appear to reproduce the general features of β-sheets found in intact proteins.

Origin of Cooperativity. The aim of this work was to investigate the cooperative interplay between two sets of weak interactions at the interface between the three strands of a *de novo* designed three-stranded antiparallel β-sheet (peptide 1−24). By comparison with the stability of the isolated C-terminal β-hairpin (peptide 9−24), we have shown that the population of folded structure at a given temperature is greater for the three-stranded sheet than the isolated hairpin, and in this sense we have demonstrated the cooperative stabilization of the C-terminal hairpin by the interactions of the N-terminal portion of the sequence. Thermodynamic analysis of the two peptides has shown the folding to be enthalpy-driven, in accord with organic solvents promoting secondary structure formation through hydrogen bonding (electrostatic) interactions.[70−73] However, van der Waals interactions between side chains implied by the many NOEs observed in the meander structure also suggest a possible enthalpic contribution to stability. We note, however, that previous studies have suggested that the hydrophobic effect makes little contribution to folding in this solvent system.[68,69]

What is the origin of the cooperative interaction between the various strands of the sheet? One possibility is that polarization of amide bonds can lead to enhanced electrostatic interactions between strands, as highlighted in Scheme 1. Recent *ab initio* calculations on a hydrogen bonded *N*-methylacetamide dimer support this conclusion.[75] The strength of the interaction [arrow in Scheme 1A] has been shown to increase when the amide groups of the dimer are effectively "solvated" by interactions with other amide groups [Scheme 1B]. The authors highlighted the implications of their calculations in the context of stabilizing effects in multiply stranded β-sheets. In the present context, hydrogen bonds between strands S3 and S2 of our three-stranded β-sheet have the potential, through this polarization mechanism,

Scheme 1

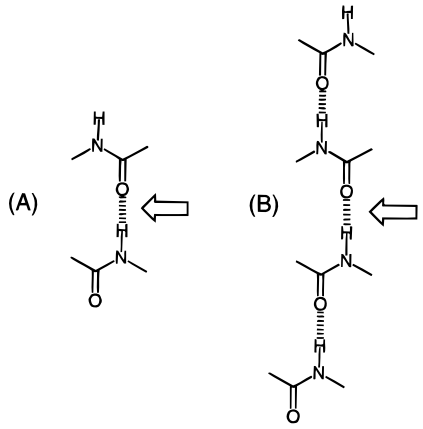

to strengthen interactions between donors and acceptors at the interface between strands S2 and S1.

The observation that glycopeptide antibiotic dimerization is promoted by the binding of model cell wall peptides has been rationalized in similar terms,[1−3,14] where the complex (ligands and antibiotic dimer) can be regarded as analogous to a multiply stranded β-sheet. Recent experimental measurements in organic solvents, from a host−guest system, also support a bond polarization mechanism for enhancing a binding interaction in a ternary complex.[76]

In the glycopeptide system, electrostatic interactions, involving antibiotic amide NHs hydrogen bonded to a ligand carboxylate group, have been shown to be cooperatively enhanced by the restriction of local motion as an increasing number of other hydrogen bond partners, or hydrophobic interactions, in close proximity help to anchor the ligand in the antibiotic binding site.[22,23,74] Thus, local steric interactions between neighboring residues imposed by an extensive framework of weak interactions are able to confine individual donor−acceptor pairs to stay in close proximity such that shorter mean hydrogen

(75) Guo, H.; Karplus, M. *J. Phys. Chem.* **1994**, *98*, 7104−7105.

bond lengths can lead to energetically more favorable interactions, providing an enthalpic component to the familiar chelate effect.[74] Such a scheme is relevant in the present context; interaction between strands S3 and S2 can be envisaged to restrict the conformational freedom of the peptide backbone such as to pre-order or template the interaction of S2 with S1. This leads to both an entropic and enthalpic enhancement to the interaction between the two strands over those interactions in the isolated β-hairpin. The entropic advantage expected from the template model is evident from the data in Table 2.

Recent estimates of the free energies of peptide hydrogen bond formation in native protein structures[77−79] have suggested that the net free energy change may be close to zero. Sippl et al.[77] have proposed that hydrogen bond formation or disruption is hindered by a barrier that provides a molecular locking mechanism that acts as a kinetic trap. Once formed, such a lock is proposed to keep the protein chain in a well-defined orientation allowing the optimization of energetically favorable side chain interactions. The key point elucidated by this model is that side chain interactions drive folding and stabilize structures, but that these interactions are mediated by the hydrogen bonding network that holds them in close proximity.[77] Clearly, the three-stranded sheet structure described in this study is considerably more dynamic and less stable than a β-sheet restrained by tertiary packing interactions in a fully folded protein. The significance of the Sippl model from the point of view of the origin of the cooperative interactions described in this work is that the size of the barrier to disruption of protein secondary structure depends strongly on local steric effects, which in turn are likely to correlate with the total number of hydrogen bonding and side chain−side chain interactions in the extended β-sheet framework; it is impossible to disrupt one interaction in the middle of a β-sheet without affecting all those that are cooperatively linked to it. In this context, local steric effects are equally likely to arise from interstrand interactions although the residues concerned may be separated by a considerable number of peptide bonds. Thus, although the difference in stability of the three-stranded sheet (1−24) versus hairpin (9−24) described in this work seems to be relatively small ($\Delta\Delta G° \approx 3$ kJ mol^{-1} at 298 K), such a model suggests that the sheet should form a more ordered structure, not on account of its greater stability, but as a consequence of the larger barrier to its disruption. Does this hypothesis fit with the experimental data? It certainly seems to, in that we see many main chain Hα and NH NOEs that strongly suggest a regular hydrogen bonding framework for the three-stranded sheet that is not evident for the isolated C-terminal hairpin. Further, many more side chain interactions (NOEs) are apparent for the sheet that seem to reflect this persistent hydrogen bonded framework. Despite the greater abundance of apparently structure-stabilizing interactions, these favorable contributions to $\Delta G°$ for folding are largely offset by the more adverse entropic cost of having a more conformationally constrained structure. Enthalpy−entropy compensation[74] results in a relatively small difference in stability between the three-stranded β-sheet and the isolated C-terminal β-hairpin.

In conclusion, the experimental conditions proved ideal for monitoring the cooperative effects described above; both the hairpin and meander structures have only marginal stability, allowing even small perturbations to conformational equilibria between folded and unfolded states to be readily detected, particularly by measurable changes in NMR parameters.

Acknowledgment. We thank BBSRC for providing support to G.J.S. and gratefully acknowledge grants from The Nuffield Foundation, The Royal Society and the support of The Department of Chemistry of the University of Nottingham. We are also grateful to John Keyte for solid phase peptide synthesis and for access to HPLC facilities in the School of Biomedical Sciences, University of Nottingham.

JA9705405

(76) Bisson, A. P.; Hunter, C. A.; Morales, J. C.; Young, K. *Chemistry*, a European Journal, in press.

(77) Sippl, M. J.; Ortner, M.; Jaritz, M.; Lackner, P.; Flockner, H. *Folding Design* **1996**, *1*, 289−298.

(78) Yang, A. S.; Honig, B. *J. Mol. Biol.* **1995**, *252*, 366−376.

(79) Yang, A. S.; Honig, B. *J. Mol. Biol.* **1995**, *252*, 351−365.